Structural Consequences of Binding of UO_2^{2+} to Apotransferrin: Can This Protein Account for Entry of Uranium into Human Cells?

Claude Vidaud,*,‡ Samuel Gourion-Arsiquaud,§,|| Françoise Rollin-Genetet,‡,|| Caroline Torne-Celer,‡ Sophie Plantevin,‡ Olivier Pible,‡ Catherine Berthomieu,⊥ and Eric Quéméneur‡

CEA Valrhô, Service de Biochimie post génomique et de Toxicologie Nucléaire, DSV/DIEP, BP17171, F-30207 Bagnols-sur-Cèze, France, and CEA Cadarache, Laboratoire de Bioénergétique Cellulaire and Laboratoire des Interactions Protéine-Métal, DSV/DEVM, UMR 6191 CNRS-CEA-Université Aix-Marseille II, F-13108 Saint Paul-lez-Durance Cedex, France

Received September 19, 2006; Revised Manuscript Received December 18, 2006

ABSTRACT: It has been established that transferrin binds a variety of metals. These include toxic uranyl ions which form rather stable uranyl-transferrin derivatives. We determined the extent to which the iron binding sites might accommodate the peculiar topographic profile of the uranyl ion and the consequences of its binding on protein conformation. Indeed, metal intake via endocytosis of the transferrin/transferrin receptor depends on the adequate coordination of the metal in its site, which controls protein conformation and receptor binding. Using UV−vis and Fourier transform infrared difference spectroscopy coupled to a microdialysis system, we showed that at both metal binding sites two tyrosines are uranyl ligands, while histidine does not participate with its coordination sphere. Analysis by circular dichroism and differential scanning calorimetry (DSC) showed major differences between structural changes associated with interactions of iron or uranyl with apotransferrin. Uranyl coordination reduces the level of protein stabilization compared to iron, but this may be simply related to partial lobe closure. The lack of interaction between uranyl-TF and its receptor was shown by flow cytometry using Alexa 488-labeled holotransferrin. We propose a structural model summarizing our conclusion that the uranyl-TF complex adopts an open conformation that is not appropriate for optimal binding to the transferrin receptor.

There is extensive literature on uranium toxicity through either inhalation ingestion or injection (*1*, *2*). This is due to considerable interest in energy and military applications, but also because it is an abundant naturally occurring element, particularly found in drinking water (*3*). Its adverse effects are observed in several target organs such as kidneys, lungs, and bone, as well as liver, muscle, and nervous system (*4*−*8*). How uranium reaches and enters targets organs is still mostly unknown. At the molecular level, the binding of uranyl ion (UO_2^{2+}) to some major blood plasma proteins, including transferrin (TF),[1] has been reported (*1*, *9*−*13*). Since many reports have highlighted the high affinity of TF for uranyl, one may invoke receptor-mediated uptake of TF-bound uranium as a possible pathway for the entrance of this toxic ion into the cells.

Transferrin changes conformation from an open to a closed conformation when binding to iron (*14*−*19*). Structural data are available for different transferrins (*20*−*24*). These 670−700-amino acid glycoproteins (80 kDa) display two structurally related but slightly different lobes called N and C lobes, both dividing into two dissimilar subdomains: N1 and N2, and C1 and C2 (*25*−*27*). Each lobe carries a well-described Fe^{3+} binding site where iron is octahedrally coordinated by two tyrosines, one monodentate aspartate, one histidine, and a bidentate synergistic carbonate ion (*16*, *18*, *25*, *28*, *29*). When iron binds, C and N lobes can reversibly convert from "open" to "closed" conformations. In a complex system of regulation (*30*−*32*), only the closed form of diferric TF (holotransferrin) displays the ability to bind transferrin receptor 1, leading to metal uptake via endocytosis (*18*, *26*, *31*, *33*−*39*).

TF coordinates a wide variety of di-, tri-, and tetravalent cations, from transition metals to lanthanides or actinides (*11*, *25*, *28*, *40*). The roles of ion geometry, size, charge, and Lewis acidity have been studied with the aim of rationalizing binding properties (*41*−*45*). Canonical metal-bound conformations are not always observed (*46*, *47*), with a negative impact on the TF−receptor recognition process (*16*, *40*, *43*, *47*, *48*). This might lead to a different metabolic fate for these metals in the organism.

In fact, little is known about uranyl binding sites in TF, and in proteins in general. These sites are difficult to predict

* To whom correspondence should be addressed: CEA Valrhô, Service de Biochimie post génomique et de Toxicologie Nucléaire, DSV/DIEP, BP17171, F-30207 Bagnols-sur-Cèze, France. Telephone: (33) 4 66 79 67 62. Fax: (33) 4 66 79 19 05. E-mail: claude.vidaud@cea.fr.

‡ CEA Valrhô.

§ Laboratoire de Bioénergétique Cellulaire, CEA Cadarache.

|| These authors contributed equally to this work.

⊥ Laboratoire des Interactions Protéine-Métal, CEA Cadarache.

[1] Abbreviations: TF, transferrin; holoTF, holotransferrin; ATR, attenuated total reflectance; FTIR, Fourier transform infrared spectroscopy; DSC, differential scanning calorimetry; CD, circular dichroism; T_m, melting temperature.

10.1021/bi061945h CCC: $37.00
Published on Web 02/01/2007

from the analysis of other TF-bound metal ions since uranium has no direct chemical equivalent. This actinide has a strong tendency to hydrolyze in aqueous medium, where it is mostly found in the form of a hexavalent uranyl dioxocation (UO_2^{2+}). As a hard Lewis metal ion, it mainly reacts with oxygen atoms, displaying a bipyramidal geometry with the two oxo groups at the tops and five- to six neighbor ligands in the equatorial plane (*49*). Its speciation at pH 7.4 in near-physiological buffer is complicated, because UO_2^{2+} forms many different stable complexes with small ligands (*50*−*52*). Using time-resolved fluorescence spectroscopy, Scapolan et al. (*10*) showed that uranium was able to bind to TF with a conditional thermodynamic equilibrium constant of $\sim 10^{16}$. However, this very high association value contrasts with the rapid dissociation observed during gel filtration experiments (*12*). The coordination environment around uranyl in TF is still unknown, and the resulting protein conformation has therefore not been described.

In this work, we first determined the protein ligands involved in UO_2^{2+} binding using UV−vis and a new application of attenuated total reflection-Fourier transform infrared difference (ATR-FTIR) spectroscopy coupled with the use of a microdialysis system (*53*). The impact of uranyl binding on the protein's conformation and thermal stability was then analyzed by circular dichroism (CD) spectroscopy and differential scanning calorimetry (DSC). In addition, we probed uranyl-TF recognition by the TF receptor of human erythroleukemia K562 cell lines. The obtained data shed light on the question of TF/TF receptor endocytosis-mediated uranium uptake.

MATERIALS AND METHODS

Materials. Purified human serum apoTF was purchased from Sigma Chemical Co. The apoTF concentration was determined from the absorbance at 278 nm using 93 000 M^{-1} cm^{-1} as a molar extinction coefficient (*54*). All chemicals were reagent grade.

The preparation of uranyl solutions required specific care to prevent metal hydrolysis and limit the incidence of speciation variations during spectroscopic and calorimetric studies. Uranyl diacetate dihydrate was dissolved in pure water (Direct-Q, MILLIPORE, 18 MΩ.cm) to create a 0.1 M stock solution (pH 4−4.5). Working solutions were prepared extemporaneously by a first dilution (1/60 or 1/120) in 10 mM sodium acetate followed by dilutions into specific buffers depending on the experiment to be performed. The final pH of each uranyl-buffered solution was also adjusted just before use at 7.4 with either HCl or NaOH.

Spectroscopic Analyses. UV−visible spectra were recorded on a Carry 300 spectrophotometer (Varian). Samples of apoTF (580 μL) were titrated at room temperature. The protein was dialyzed prior to use, and concentrations were within the range of ∼12.5 μM for UV studies and ∼75−85 μM for visible studies. The appropriate buffers were used for background correction from 200 to 600 nm. Depending on the experiments, 1−10 μL uranyl aliquots were added and mixed either in both sample and reference cells or only in the sample cuvette. The equilibration time required for metal−protein binding was 10 min, but solutions were allowed to equilibrate for 20 min after each titrant addition where data were recorded. At the end of the experiments, volume variations did not exceed 5% of the total volume. The differential spectra were generated by mathematical subtraction between the modified and initial spectra of the apoprotein. To normalize the results, the absorbance variations at 242 nm (or 400 nm) were divided by the total transferrin concentration to give $\Delta\epsilon$, the apparent absorbtivity at each wavelength. Titration curves were prepared by plotting $\Delta\epsilon$ versus the ratio of total uranyl molar concentration to total transferrin molar concentration (U/TF). The reported results are the average values taken from two titrations.

CD Spectra. Spectra were recorded on a J-810 spectropolarimeter (Jasco, Tokyo, Japan). The apoTF (∼16 μM) was dialyzed against 50 mM Hepes, 150 mM NaCl, and 1.7 mM sodium acetate (pH 7.4) prior to use. The protein solution was then distributed in assay samples (500 μL) before addition to each sample of 1−10 μL of 10 mM uranyl solutions in the same buffer without NaCl. Measurements were recorded between 230 and 600 nm in 10 mm cells, at 20 °C after equilibration for at least 20 min. Each spectrum is the sum of at least three scans, after baseline subtraction. All CD spectra were normalized on the basis of protein concentration. The reported results were confirmed twice.

Microdialysis Coupled to ATR-FTIR. We modified the microdialysis ATR system described in ref *53* to allow the analysis of high-affinity metal-binding sites. The perfusion on the protein sample, of two buffers differing only by the presence of the metal, allows the recording of "metal-bound" minus "metal-free" FTIR difference spectra. After such a metal binding cycle, a metal-chelating buffer was perfused through the sample to remove the metal. Therefore, the Flow-Thru unit of the ATR device (*SensIR* Technologies) was connected via silicone tubings to a peristaltic pump and two electronically controlled three-way valves, in series, allowing the selection of one of three possible buffers. Two microliters of a 1.5 mM apoTF solution in 20 mM Tricine and 10 mM $KHCO_3$ (pH 8) (TC buffer) was deposited on the diamond prism. Sample absorption reached 0.8 absorption unit at 1640 cm^{-1}. A dialysis membrane (Spectra/Por membrane with a MWCO of 35 000) was deposited on the sample and maintained between the Flow-Thru unit and the diamond crystal using a 0.2 mm thick O-ring. To analyze binding of iron to apoTF, the concentrated protein sample was equilibrated by the continuous flow of the metal-free Tricine buffer containing 50 μM sodium citrate and 10 mM bicarbonate. When the FTIR absorption spectrum of the sample was stable, a single-beam spectrum was recorded ("free Fe" spectrum, Fe_f), and the flowing solution was switched to a Tricine buffer containing 50 μM iron citrate. A perfusion delay of 6 min was optimized to allow equilibration of the sample in the presence of iron. After this delay, a single-beam spectrum corresponding to the TF-bound Fe (Fe_b) was recorded. The FTIR difference spectrum showing the absorption changes induced by binding of iron to TF was given as the difference between the two single-beam spectra ($Fe_b - Fe_f$). A third buffer consisting of 20 mM sodium citrate and 0.1 mM EDTA (pH 5) was then passed through the sample to deplete the protein from the iron. This buffer was perfused for 5 min, after which the flowing solution was switched to the iron-free Tricine buffer. Single-beam spectra were recorded before and at various times after treatment for 5 min with the citrate/EDTA buffer, to verify that the

subsequent perfusion of iron-free buffer allowed complete equilibration of the iron-free TF at the proper pH. Thus, only IR changes associated with iron release are detected in the following $Fe_f - Fe_b$ difference spectra.

Binding of UO_2^{2+} to apoTF was analyzed in 50 mM Hepes (pH 7) containing either 40 μM Na acetate or 20 μM UO_2^{2+} acetate. A 30 mM phosphate buffer at pH 5 was used to deplete TF from uranyl. The equilibration times were the same as those optimized for the iron binding experiments.

FTIR Spectroscopy. The FTIR spectra were recorded at 4 cm^{-1} resolution, on a Bruker IFS28 spectrometer equipped with DTGS or MCT-A detectors. All frequencies quoted are accurate to ± 1 cm^{-1}. Three hundred interferograms were averaged for each single-beam spectrum. Typically, one reduction−oxidation cycle lasted for 20 min. Spectra from ~40 consecutive metal binding cycles were accumulated for each sample, and the results obtained with three to five samples were averaged.

Calorimetric Measurements. Microcalorimetric measurements were carried out with a high-sensitivity differential scanning VP-DSC microcalorimeter (MicroCal Origin Software) with a 0.51 mL cell at heating rates of 85 K/h. All solutions were first degassed in a vacuum prior to loading. The solutions were prepared by incubation of apoTF (17−20 μM) with different uranyl molar ratios for 24 h at room temperature in 50 mM Hepes and 1.7 mM acetate (pH 7.4) supplemented with 1.2 mM bicarbonate. These buffers were chosen for their low temperature sensitivity (small dpH/dT) and their capability of uranyl solvation. The heating curves were corrected for the baseline obtained by heating the solvent alone. DSC scans were performed on identical samples at different scan rates or at different concentrations to determine any dependency of the shape of the transition peak on these temperature ramps or on concentration.

Flow Cytometry Analysis. UO_2^{2+}-loaded TF species were prepared by mixing UO_2^{2+} acetate and an apoTF solution in a molar ratio of 2/1. The reaction was followed by spectrophotometry as previously described to control the saturation of the protein. Human erythroleukemia K562 cells (ATCC number CCL-243) were cultured in RPMI 1640 (Invitrogen) supplemented with 10% inactivated bovine serum (Hyclone) and 100 units/mL penicillin and streptomycin (Invitrogen) at 37 °C in a 5% CO_2 atmosphere. Briefly, as described by Du et al. (*55*), experiments were performed with a cell density of $\sim 5 \times 10^5$ cells/mL. The competitive effect of uranyl-TF species on binding of holoTF to K562 cells was studied by flow cytometry and compared to those of apotransferrin and holotransferrin. The solutions with a constant concentration of Alexa 488-labeled holoTF (T13342, Invitrogen) and various concentrations of unlabeled holoTF, apoTF, and uranyl-TF were each incubated with a K562 cell suspension (10^6 cells/mL) for 30 min in 10 mM Hepes buffer (pH 7.4) and 0.15 M NaCl at 37 °C. After the samples had been chilled for 30 min at 4 °C, centrifuged at 500*g* for 5 min, and washed, the fluorescence intensity of each cell was recorded on a FACSCalibur flow cytometer (Becton-Dickinson) with an argon laser set at a λ_{ex} of 488 nm and a λ_{em} of 530 ± 15 nm. The fluorescence intensity was obtained by integrating the intensity per cell from $\sim 4 \times 10^4$ cells for each sample.

RESULTS

UV−Vis Spectroscopic Studies. UV−vis spectroscopy represents a simple and powerful way to monitor the interactions between UO_2^{2+} and TF. However, uranyl undergoes a slow re-equilibration when a high concentration solution is mixed into a diluting buffer, even in the absence of protein. This impeded fast measurements since absorption spectra were shown to evolve for ~20 min under our experimental conditions, giving rise to a regular decrease in absorbance in the 240−480 nm region (data not shown). This effect was attributed to the strong tendency of UO_2^{2+} to form hydroxides at near-neutral pH and to slow equilibrium rates of some UO_2^{2+} complexes with buffer components such as acetate or carbonate. The complex speciation of uranyl ions in biochemical media has been the subject of many previous reports (*9*, *51*, *52*). We used the J Chess algorithm to calculate the distribution of uranyl species under most buffer conditions used in this study (data not shown). It appeared that whatever buffer system was used, uranyl exists mostly as $(UO_2)_2CO_3(OH)_3$.

To avoid spectral distortion due to the changes in UO_2^{2+} speciation upon simple dilutions, two experimental setups were used for the accurate determination of the uranyl-TF saturation curve by UV−visible spectrophotometry,

Specificity of Uranyl-TF Binding. In a first set of experiments, uranyl acetate was added simultaneously to both sample and reference spectrophotometer cuvettes. Series of UV spectra could be collected for a range of U/TF molar ratios of 0−7 (Figure 1). Major spectral changes occurred at 240−245 and 290−300 nm, indicating the deprotonation of some tyrosine phenolate groups as previously described (*16*, *25*, *56*). A modification in the visible region of the spectrum (330−430 nm) was also observed.

Metal binding was titrated at 242 nm, and a representative set of experiments is given in Figure 1 (inset). The presence of low concentrations of acetate or carbonate in the buffers was necessary to prevent the formation of U-hydroxide species that tended to precipitate. Whatever buffer composition was used, similar curves were obtained. Absorptivity increased quasi-linearly up to a uranyl/protein molar ratio (U/TF) of ~1 and beyond, which indicates that uranyl is binding to more than one site in apoTF. All titration curves reached a plateau of approximately 22 000 M^{-1} cm^{-1} when the U/TF molar ratio exceeded 2. Using time-resolved fluorescence, Scapolan et al. (*10*) measured a ratio of 2. In a previous nonquantitative study, we already observed a ratio of ~1.6 uranyl per TF by ICPS-MS, but after gel filtration (*57*). We confirmed a stoichiometry of 2 UO_2^{2+} ions per TF by spectroscopic measurements in the visible region (400 nm), where apoTF does not absorb and where UO_2^{2+} species present a weak absorption band in the 335−480 nm region. A higher protein concentration was thus required (75 μM), and a slight yellow color was observed upon addition of uranyl. Again the initial part of the curve was quite linear and reached a plateau at ~2 uranyl ions per protein (Figure 1, inset).

From this first set of experiments, we considered that below TF saturation, all UO_2^{2+} cations were specifically bound to TF and, therefore, that absorption variations due to speciation changes of the "free" remaining UO_2^{2+} could be neglected.

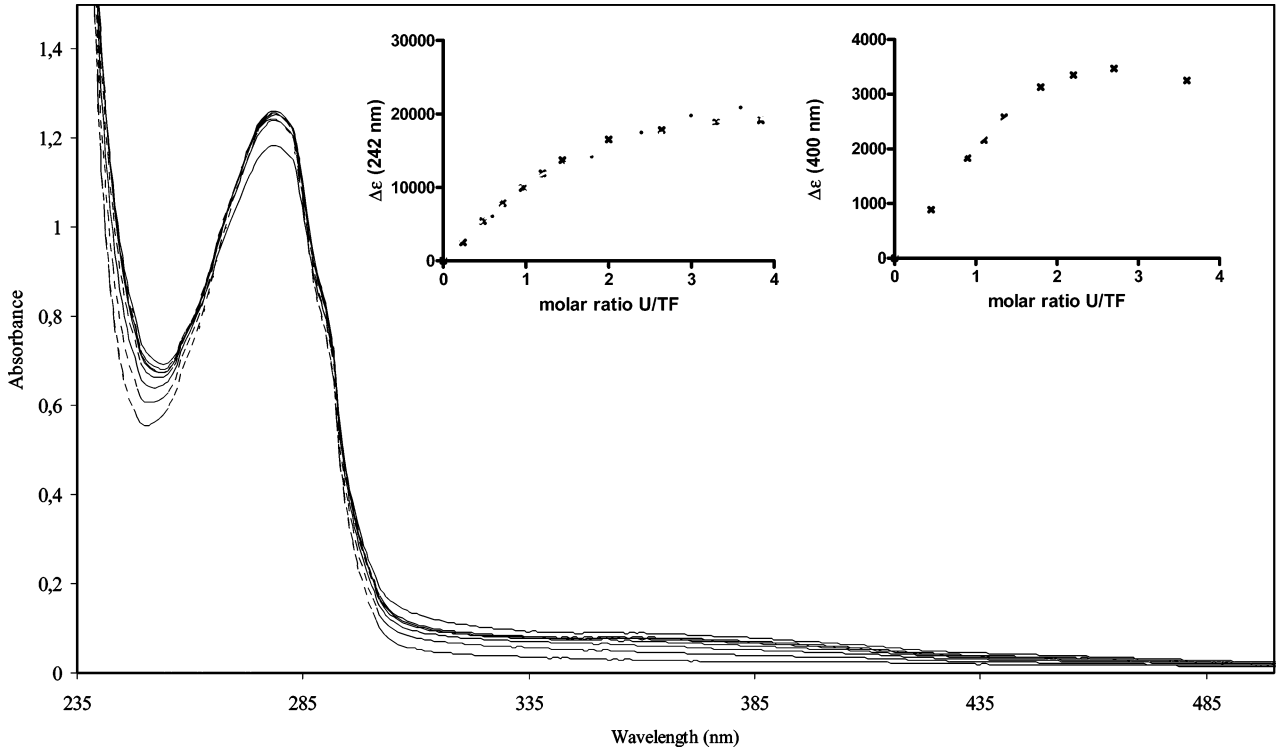

FIGURE 1: UV−vis saturation spectra of apoTF with uranyl acetate. ApoTF in 150 mM NaCl, 1.7 mM sodium acetate, 50 mM Hepes buffer at pH 7.4. Uranyl diacetate was added to both cells. Spectra were registered after equilibration for 20 min. From bottom to top: addition of uranyl acetate at UO_2^{2+}/apotransferrin (U/TF) ratios from 0 to 7. The inset shows transferrin saturation curves with uranyl acetate at 242 (left) and 400 nm (right). Absorptivity plots of $\Delta\epsilon$ vs UO_2^{2+}/apotransferrin (U/TF) ratios are reported.

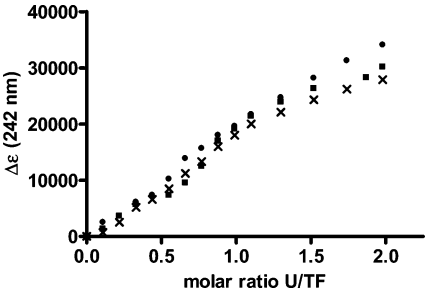

FIGURE 2: Titration curves for the addition of uranyl acetate to apotransferrin. Spectra were registered after equilibration for 20 min. Absorptivity plots of $\Delta\epsilon$ vs UO_2^{2+}/apotransferrin (U/TF) ratios are reported. Uranyl diacetate was added only to apoTF in 50 mM Hepes, 150 mM NaCl buffers (pH 7.4) at different acetate and carbonate concentrations: (●) 0.2 mM acetate, (■) 0.2 mM acetate and 0.3 mM carbonate, and (×) 0.3 mM carbonate and 1.7 mM acetate.

Determination of the Number of Tyrosines Involved in Binding. Indeed, the subtraction of absorption changes in the reference cuvette with UO_2^{2+} in solution might have led to an underestimation of absorptivity at 242 nm. So, in the second set of experiments, the uranyl solution was only added to the sample cell. The absorption associated with tyrosine−metal coordination was again recorded at 242 nm. A representative set of titration curves is shown in Figure 2. Linear regression to a U/TF of 1 confirmed the expected proportionality between addition and consumption of UO_2^{2+} by the protein. As a result, the average slope equaled the molar absorptivity of the uranyl-TF complex at 242 nm, i.e., 18 000 ± 2000 M^{-1} cm^{-1}. Considering an absorptivity of 8000−9000 M^{-1} cm^{-1} per metal-bound tyrosine (*58*), two tyrosines would be involved in UO_2^{2+} binding at a first site. The linear portion extended to a U/TF ratio of ∼1.5, which confirmed that the metal bound to two sites in apoTF, probably the two iron binding sites, and with similar affinities. On the basis of this value, one would expect saturation of the protein with two uranyl ion equivalents to produce an absorptivity of 36 000 M^{-1} cm^{-1} at 242 nm. A slight curvature was observed between U/TF ratios of 1.5 and 2, indicating either weaker binding at the second UO_2^{2+} binding site or competitive binding from hydroxide, acetate, or carbonate for the UO_2^{2+} ion in the buffer. For a U/TF ratio of 2, the curves reached 30 000 ± 2000 M^{-1} cm^{-1} corresponding to ∼3.5 tyrosinate equivalents involved in binding. These spectroscopic data are consistent with uranyl binding at two sites, each involving two tyrosines.

To further analyze the binding mode of UO_2^{2+} in apoTF, and to determine whether it involves the tyrosine residues from the iron binding site, we identified the IR signatures of the iron ligands in FTIR difference spectra associated with Fe^{3+} binding and compared them with signatures of the UO_2^{2+} ligands (observed in the difference spectra associated with UO_2^{2+} binding).

Analysis of Binding of Iron to ApoTF by ATR-FTIR Difference Spectroscopy. The iron coordination sphere is composed of two tyrosines, one histidine, a monodentate aspartate, and carbonate as a bidentate ligand (*16*, *25*, *28*). To identify the IR signatures from the different iron ligands, we alternately perfused iron-free and iron-containing buffers on the apoTF samples using the ATR microdialysis system[2]

[2] Given the high affinity of the iron binding site in transferrin, we modified the microdialysis system described in ref *56* to allow the perfusion of the protein sample by a third buffer, containing citrate and EDTA, to extract the iron from holotransferrin before re-equilibrating the sample with the Fe-free Tricine buffer, as detailed in Materials and Methods.

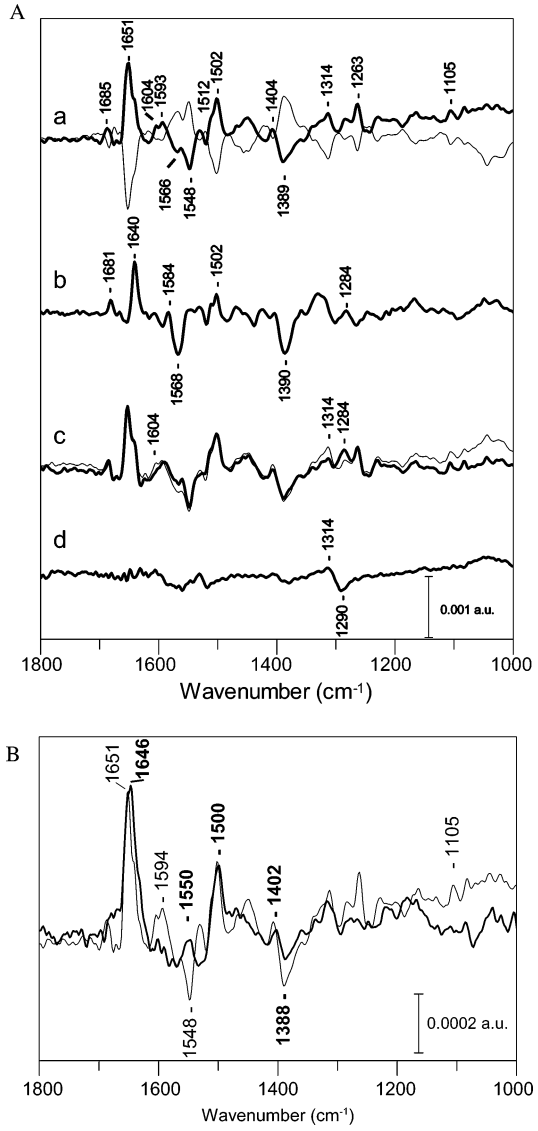

FIGURE 3: Effects of metal−TF interactions on FTIR difference spectra. (A) Effect of iron−TF interactions on the FTIR difference spectra: (a) $Fe_b - Fe_f$ (thick line) and $Fe_f - Fe_b$ (thin line) spectra recorded with TF in Tricine buffer (pH 8), (b) $Fe_b - Fe_f$ spectrum recorded with deuterated apoTF sample and buffers, (c) superimposition of $Fe_b - Fe_f$ spectra recorded in the presence of ^{13}C-labeled (thick line) and ^{12}C-labeled (thin line) bicarbonate, and (d) $^{12}C - ^{13}C$ difference spectrum calculated from the spectra in part c. Only IR modes of (transferring-bound) bicarbonate sensitive to bicarbonate ^{13}C labeling are observed in this difference spectrum. (B) Comparison of the influence of binding of UO_2^{2+} and Fe^{3+} on apoTF by superimposition of $UO_{2b} - UO_{2f}$ (thick line) and $Fe_b - Fe_f$ (thin line) FTIR difference spectra.

(*53*). We registered FTIR difference spectra associated with iron binding ($Fe_b - Fe_f$) and iron release ($Fe_f - Fe_b$) (Figure 3A, thick and thin lines, respectively). The two spectra displayed a large number of highly reproducible bands and are almost mirror images one of the other, showing that the IR bands are actually due to structural changes induced by Fe fixation or release in apoTF. The band assignments were performed by classical normal-mode analysis, combined with the observation of a H−^{2}H exchange effect, in Fe binding experiments performed in ^2H_2O (Figure 3A, trace b).

In the $Fe_b - Fe_f$ spectrum, a positive band at 1502 cm^{-1} with a distinct shoulder at 1512 cm^{-1} was in the frequency range where the most intense tyrosine side chain mode [ν(CC) ring mode] is expected (*59*). The frequency of these bands remained almost unchanged at 1510 and 1502 cm^{-1} in the $Fe_b - Fe_f$ spectrum recorded in ^2H_2O (Figure 3A, trace b), supporting their assignment to the ν(CC) ring mode of two tyrosines (*59*, *60*). The two bands at 1512 and 1502 cm^{-1} were thus assigned to the two side chain modes of the tyrosine ligands of the iron.

A difference band was observed at 1389 (−) and 1404 (+) cm^{-1}, in the spectra recorded in H_2O (Figure 3A, trace a) and ^2H_2O (Figure 3A, trace b). In this region, relatively intense bands only weakly affected by H−^{2}H exchange are best explained by the symmetric stretching mode $\nu_s(COO^-)$ of a carboxylate group. The corresponding asymmetric $\nu_{as}(COO^-)$ mode is expected in the 1620−1540 cm^{-1} region. The frequency of this mode is also only slightly sensitive to H−^{2}H exchange (*59*, *60*). In this region, the negative band at 1566 cm^{-1}, slightly upshifted to 1568 cm^{-1} in ^2H_2O, is a good candidate for the carboxylate $\nu_{as}(COO^-)$ in apoTF. In contrast, the negative band at 1548 cm^{-1} (Figure 3A, trace a), largely perturbed upon H−^{2}H exchange, is assigned to the peptide ν(CN+NH) amide II mode (*61*, *62*). Thus, the bands at 1568 and 1389 cm^{-1} are attributed to the ν_{as} and $\nu_s(COO^-)$ modes of a carboxylate of apoTF, modified upon iron fixation. This carboxylate group is assigned to the side chain of the monodentate aspartate ligand of the iron.

In the FTIR spectra, a positive band is reproducibly observed at 1105 cm^{-1} (Figure 3A, trace a). The frequency of this band is typical of a histidine side chain involved in metal coordination (*53*, *63*, *64*). The small but reproducible signal at 1105 cm^{-1} is therefore assigned with confidence to the $\nu(C_5N\tau)$ mode of the histidine ligand of the iron in transferrin.

Experiments were performed using ^{12}C- and ^{13}C-labeled bicarbonate (Figure 3A, trace c) to identify the IR changes corresponding to the synergistic carbonate anion upon iron fixation. The spectra recorded with ^{12}C- and ^{13}C-labeled bicarbonate (Figure 3A, trace c) superimpose nicely except in the 1600−1500 and 1350−1250 cm^{-1} regions. These differences clearly appeared in the $^{12}C - ^{13}C$ spectrum (Figure 3A, trace d) calculated from spectra of trace c of Figure 3A. The band at 1314 cm^{-1} assigned to ^{12}C-labeled carbonate is downshifted to 1290 cm^{-1} upon ^{13}C labeling. Moreover, the carbonate ion in solution is characterized by a band at 1450−1410 cm^{-1}, while two bands are observed at 1620−1520 and 1340−1260 cm^{-1} on metal coordination (*65*, *66*). The band at 1314 cm^{-1} was thus typical for the coordinated ^{12}C-labeled carbonate $\nu_s(COO^-)$ mode (*63* and references therein).

Another large band was detected in the $Fe_b - Fe_f$ spectra of Figure 3A at 1651 cm^{-1}, in a region where the ν(C═O) mode of backbone peptide groups is expected to contribute (*61*). The downshift of this band to 1640 cm^{-1} (^2H_2O) (Figure 3A, trace b) confirmed its assignment to a peptide amide I mode. This band corresponds to a slight structural change at the level of peptide groups occurring upon iron binding in transferrin.

Binding of UO_2^{2+} to ApoTF. The spectrum corresponding to the interaction of UO_2^{2+} with apoTF is shown in Figure 3B (thick line). It is superimposed on the $Fe_b - Fe_f$ spectrum (thin line). There are many similarities between these two spectra. Given the high sensitivity of FTIR difference spectroscopy to even minute structural changes, these

similarities strongly suggest that uranyl binding occurs at the iron binding site in apoTF and involves some of the iron ligands.

The positive bands at 1512 and 1502 cm^{-1}, assigned to the side chains of the two iron tyrosine ligands, are preserved in the $UO_2^{2+}{}_b - UO_2^{2+}{}_f$ spectrum. This is a strong argument to conclude that uranyl binding involves both tyrosines at the iron binding site. In contrast, there is no equivalent in the $UO_2^{2+}{}_b - UO_2^{2+}{}_f$ spectrum of the positive band at 1105 cm^{-1} assigned to the iron histidine ligand side chain. This shows that histidine is not involved in UO_2^{2+} coordination. As for the carboxylate side chain modes of the aspartate ligand, in the $UO_2^{2+}{}_b - UO_2^{2+}{}_f$ spectrum, we observed a band at 1390/1402 cm^{-1} similar, though less intense, to that detected in the $Fe_b - Fe_f$ spectrum, while significant changes are observed in the 1620−1540 cm^{-1} region, where the $\nu_{as}(COO^-)$ mode is expected to contribute. The frequency of this $\nu_{as}(COO^-)$ mode is highly sensitive to the carboxylate environment or binding mode (*66*). These changes suggest that the aspartate environment is indeed disturbed upon uranyl binding but that the existing interactions between UO_2^{2+} and aspartate differ from those observed with Fe^{3+}.

Differences between the two spectra in the 1600−1520 cm^{-1} region and at 1320 cm^{-1} also seem to indicate that carbonate is not involved in the same interactions with Fe^{3+} and UO_2^{2+}, although we cannot exclude binding of carbonate to UO_2^{2+}.

Finally, the positive band at 1651−46 cm^{-1} observed upon UO_2^{2+} binding is similar though broader than the one detected at 1651 cm^{-1} upon Fe binding. This indicates the same perturbation of few peptide groups upon binding of both iron and UO_2^{2+} to apoTF, while an additional reorganization at a peptide carbonyl could occur upon UO_2^{2+} binding.

Circular Dichroism Analysis of the Effect of UO_2^{2+} Binding on Tertiary Structure. Metal binding to apotransferrin does not produce significant changes in the far-UV spectra that allow secondary structure modifications to be identified upon metal binding (*67*). But within the range of 230−320 nm, changes in the tertiary folding of polypeptide chains can modify the chiral environment of the aromatic side group chromophores, leading to different CD spectra.

CD spectra of apo-, holo-, and uranyl-transferrin were recorded in the near-UV region (Figure 4). They display similar shapes, with strong negative bands at 242−244 nm, and a broad negative band in the 250−280 nm region which is attributed to disulfide bonds (19 in transferrin) and induced chirality of aromatics. Above 285 nm, CD spectra of the three proteins largely differed.

For iron-saturated protein, an important Cotton effect was observed as expected within the 400−450 nm range, with a strong negative band at ~460 nm (not shown). In this region, the uranyl-saturated TF dichroic spectrum was quite different with a slight positive broad band. At ~295 nm, uranyl-TF and apotransferrin displayed the same negative band. This band could be hidden by overlapping positive absorption in the case of holoTF. In the 250−290 nm region, the spectra of apo- and uranyl-transferrin were quite superimposed while that of Fe^{3+}-TF differed. The protein tertiary structure in the vicinity of aromatic amino acids was also more modified upon binding of Fe^{3+} than upon binding of UO_2^{2+}.

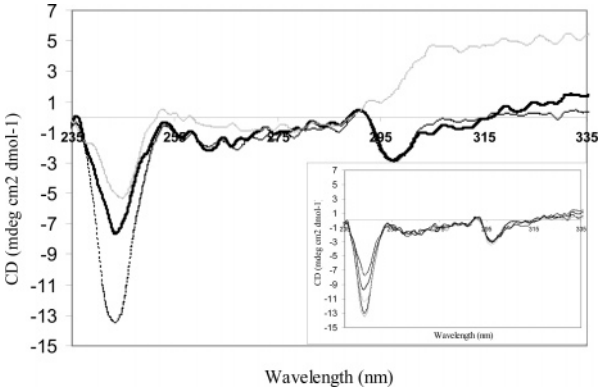

FIGURE 4: Comparison of apo-, holo-, and uranyl-TF near-UV CD spectra. Uranyl acetate (4 molar equiv) and ferric citrate (4 molar equiv) were added to apoTF in 50 mM Hepes, 1.7 mM acetate buffers at pH 7.4 and 310 K. CD spectra were recorded after 20 min: apoTF (dotted line), uranyl-saturated protein (black line), and iron-saturated protein (gray line). The inset shows CD spectra of binding of uranyl to apotransferrin. From bottom to top: addition of 0, 0.5, 1, 2, and 4 equiv of uranyl acetate to apotransferrin.

The strong negative band at ~242−244 nm was coincident with those found at 242 nm in the UV spectra for Fe^{3+} and uranyl-protein solutions. The intensity of this band was clearly dependent on uranyl binding, as shown in the inset of Figure 4. For uranyl saturation, the intensity of this band was intermediate between that of apoTF (stronger negative signal) and holoTF (weaker negative signal).

The results indicate a greater interaction and change in tyrosine environment for holoTF than for uranyl-transferrin and could then suggest differences related to lobe closure and protein stability. This was studied using differential scanning calorimetry (DSC).

Analysis of Thermodynamic Stabilities. The choice of buffers is very important for DSC experiments with regard to protein−metal interactions, but we had to accommodate uranyl speciation requirements, since it is indeed very complex and poorly described in biological buffers. We therefore chose to use similar Hepes buffer compositions in uranyl binding studies, to limit as much as possible variations in experimental conditions that could lead to different species interacting with transferrin.

Differential scanning microcalorimetry experiments were carried out with apoTF and different degrees of ferric citrate or uranyl acetate saturations. We first recorded reference thermograms upon binding of iron to apoTF. Due to a stronger metal affinity for the C site, the mechanism of binding of iron to TF is sequential (Figure 5A). As reported in the literature, the C site was first saturated by gradual addition of Fe^{3+} with a melting temperature (T_m) shift from 57.5 to 88.2 °C. The N site transition, which has the lower T_m after C saturation by iron, was then stabilized by a high-energy pairwise interaction (ΔG_{C-N}) between the N and C lobes (*68*). Final stabilization of the N site occurred on saturation with Fe^{3+} at a higher final T_m (88.2 °C). Lin et al. (*69*) reported that the melting transition of the N and C lobes of TF can each be described as a single two-state transition model, associated with symmetrical peaks in the unfolding curve.

DSC thermograms in the presence of uranyl ions were completely different (Figure 5B). The initial scan of apotransferrin in 50 mM Hepes and 1.7 mM acetate at pH 7.4

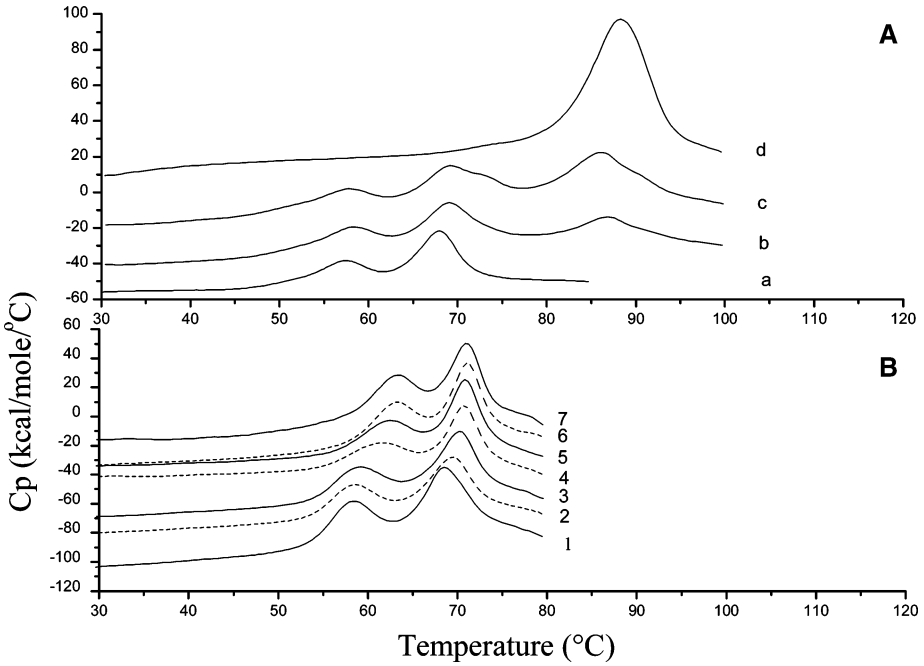

FIGURE 5: DSC thermograms of holo- and uranyl-transferrin. (A) DSC scans of apotransferrin saturated with different Fe^{3+}/apotransferrin ratios. Scans were performed in 50 mM Hepes buffer at pH 7.4: (a) apotransferrin, (b) partially saturated C site, (c) C site saturation and N site stabilization, and (d) iron-saturated transferrin. (B) DSC scans of apotransferrin saturated with different UO_2^{2+}/apotransferrin ratios. Scans were performed in 1.7 mM acetate, 50 mM Hepes buffers at pH 7.4. The apotransferrin concentration ranged from 17 to 20 μM: curve 1, apotransferrin; and curves 2−7, 0.2, 0.4, 0.8, 2, 4, and 8 mol of uranyl acetate/mol of apotransferrin in the DSC cell. Thermograms were performed at 85 K/h.

presented two independent transitions, with two T_m values of 58.0 (C site) and 68.4 °C (N site). Two successive scans of uranyl-transferrin complexes were carried out from 25 to 73 °C, leading to the same thermograms (data not shown). By measuring the uranyl-transferrin concentration before the first scan and after the second one, we found more than 75% reversibility. Precipitation occurred after 75 °C and could macroscopically be observed with a great effect on the variation of the calorimetric enthalpy (ΔH_{cal}), preventing the calculation of ΔC_p. Then we tested kinetically determined irreversible processes, such as aggregation, because they can affect the shape of the thermograms and are dependent on scan rate. We checked different scan rates from 45 to 85 K/h for the apotransferrin-uranyl complex in this buffer (data not shown). The same T_m values were found at each scan rate, indicating that protein denaturation was not kinetically controlled. Thus, the recorded data were considered to relate to reversible change prior to final aggregation (*70*).

The thermodynamic data for C and N site stabilization are given in Table 1. Upon uranyl binding, the scans showed progressive protein saturation by the metal, leading to its stabilization (T_m higher than in the apo form of the protein); uranyl caused selective perturbation, and for a U/TF ratio of less than 0.8, the T_m values of both sites were simultaneously increased, from 58.0 to 61.5 °C for the C domain and from 68.4 to 70.7 °C for the N domain. Above a U/TF ratio of ~0.8, the C site T_m still increased slightly from 61.5 to 63.3 °C while the N site T_m was stabilized at 71 °C.

Whatever the U/TF ratio, we could conclude that in the case of uranyl binding only weak differences in the T_m values were observed between apoTF and uranyl-bound transferrin. This indicates weak modifications in both protein stability and protein conformation close to the apo form of the protein. These DSC results led us to two different hypotheses: either

Table 1: Thermodynamic Parameters in the Uranyl-ApoTF Binding Reaction[a]

initial uranyl/apotransferrin molar ratio	T_m (°C)	
	first transition	second transition
0	58.0 ± 0.36	68.4 ± 0.39
0.2	59.0	69.3
0.4	59.4 ± 0.23	70.2 ± 0.20
0.8	61.5	70.7
2	62.6 ± 0.14	70.8 ± 0.06
4	63.2 ± 0.03	71.1 ± 0.05
8	63.3 ± 0.07	70.9 ± 0.05

[a] All solutions were first degassed in a vacuum prior to loading. Protein concentrations varied from 17 to 20 μM. Experiments were performed in 50 mM Hepes, 1.7 mM acetate, and 1.2 mM carbonate at pH 7.4. Data from three or more replicate experiments were averaged; standard deviations are given. Other values are averaged from two replicate experiments.

similar affinities for both sites or a slightly higher affinity for the N site. However, the UV−vis experiments (Figure 1) showed a single slope above one uranyl ion per protein and then no large difference between the two sites, suggesting very similar interactions. Since our major result was the evidence for an incomplete lobe closure, an additional confirmation of the simultaneous interactions by other studies was less important in our study. Therefore, we focused on the biological consequence of this biochemical fact, looking at transferrin receptor recognition and endocytosis.

Uranyl-TF−Transferrin Receptor Interaction. The binding of Alexa 488-labeled holoTF to K562 cells was first evaluated by flow cytometry (Figure 6A). Saturation was reached at 0.3 μM labeled holoTF. Competition with different ratios (20/1, 10/1, 5/1, 2/1, 1/1, and 0.1/1) of uranyl-TF, apoTF, and holoTF versus labeled holotransferrin was followed after incubation for 30 mn at 37 °C. As expected

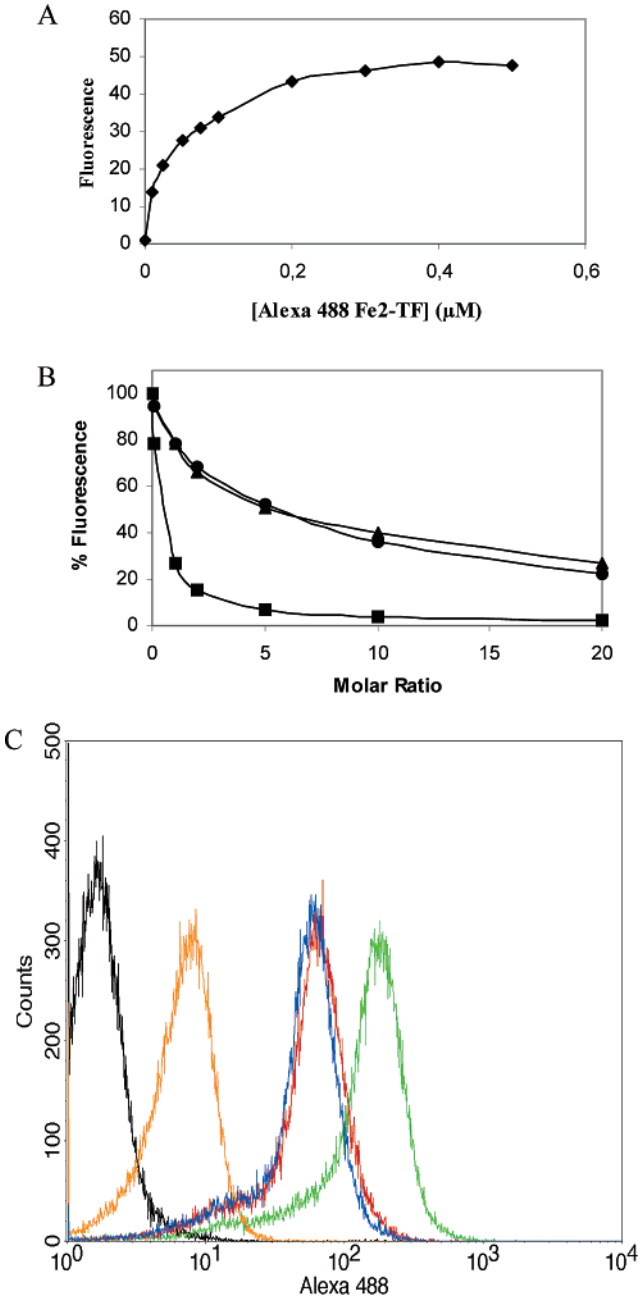

FIGURE 6: Binding of uranyl-TF to K562 cells. (A) Saturation curve for binding of Alexa 488-labeled holoTF to K562 cells. Fluorescence (geometric mean) of K562 cells vs Alexa 488-labeled holoTF concentration; $\lambda_{ex} = 488$ nm, and $\lambda_{em} = 530 \pm 15$ nm. (B) Inhibition of the cellular fluorescence of binding of Alexa 488-labeled holoTF (0.3 μM) to K562 cells by different concentrations of uranyl-TF (▲), apoTF (●), and holoTF (■); results are expressed as the percent of the initial fluorescence. (C) Histograms of K562 fluorescence: negative population (black) and the cell population after incubation with 0.3 μM Alexa 488-labeled holoTF (green) as a control and with 10/1 apoTF (blue), uranyl-TF (red), or holoTF (orange).

(Figure 6B), only holoTF inhibited ~60% of the Alexa 488 fluorescence signal with a 1:1 molar ratio. Apo- and uranyl-TF displayed the same inhibition profile, demonstrating that no or otherwise very weak binding occurred at stoichiometric concentrations. In the presence of a uranyl-TF/labeled holoTF ratio of 10/1, the cell population is slightly shifted to a lower fluorescence level similar to that observed with the same apoTF/labeled holoTF ratio (Figure 6C). Even uranyl-TF/holoTF ratios of 20 did not lead to complete fluorescence inhibition, and hence inhibition of holoTF−TF receptor interaction. These results indicate that uptake of uranyl-TF by transferrin receptors and the endocytosis mechanism are most probably ineffective under physiological conditions, where the level of available apotransferrin does not exceed 60% of total transferrin.

DISCUSSION

Apotransferrin was shown to bind two uranyl ions, and the conditional thermodynamic constant (K) was previously determined to be 10^{16} (*9*). This raised the question of the possible involvement of the TF/TF receptor system in uranyl uptake. This mechanism would necessitate a closed uranyl-TF conformation for transferrin recognition. In this study, we analyzed UO_2^{2+} binding sites in transferrin and evaluated the subsequent structural changes, notably lobe closure and stability modifications.

From UV−visible spectrophotometry, we confirmed that apotransferrin indeed binds two uranyl ions. Absorptivities detected upon uranyl binding on typical tyrosinate metal absorption indicated that four tyrosines (two per site) are involved as uranyl ligands. These tyrosines are generally assumed to be located at the apotransferrin iron binding sites (*16*, *40*). FTIR was therefore used to compare the UO_2^{2+} and Fe^{3+} binding sites. IR signatures of the Fe^{3+} ligands were identified. The IR signature of the two tyrosines involved in each Fe^{3+} binding was also detected upon uranyl-TF interaction. This demonstrated that they participate in the UO_2^{2+} coordination sphere, in line with the UV−vis results. In contrast, we did not detect IR contributions from the side chain of the histidine iron ligand in the presence of UO_2^{2+}, ruling out the participation of His249 with the coordination sphere of UO_2^{2+}. We also concluded from the FTIR experiments that there are different interactions of either iron or uranyl with aspartate and carbonate. From these data, and considering the iron binding site structure, we propose a binding model for uranyl in which the tyrosines are in the equatorial plane, while the uranyl oxos are located on a perpendicular line excluding histidine and involving at least one carboxylate oxygen from the coordination sphere.

His249 mutations weaken the iron binding ability, and desalting the corresponding mutated holotransferrin on gel filtration columns removes half the iron from the proteins (*71*, *72*). A loss of uranyl ions was also observed for uranyl-TF under similar experimental conditions (*7*). His249 and Asp63 ligands contribute to the movement required for lobe closure (*17*). It has also been proposed that the lack of binding of iron to His585 in the C lobe might preclude binding of iron to Asp392 (*73*). The lack of UO_2^{2+} interaction deduced from the His IR signal and perturbation of the Asp coordination should hinder complete lobe closure upon uranyl binding. Near-UV CD spectral analysis confirmed that the tertiary structure of the protein was less affected by UO_2^{2+} than Fe^{3+} binding, in line with partial lobe closure.

DSC results supported the assumption that domain closure was not complete and that uranyl-TF was less stable than holoTF. The mechanism of sequential binding of iron to TF associated with important shifts in T_m was not observed at all upon uranyl interaction. Melting transitions of C and N

Scheme 1: Proposed Structural Model of Metal Binding in TF[a]

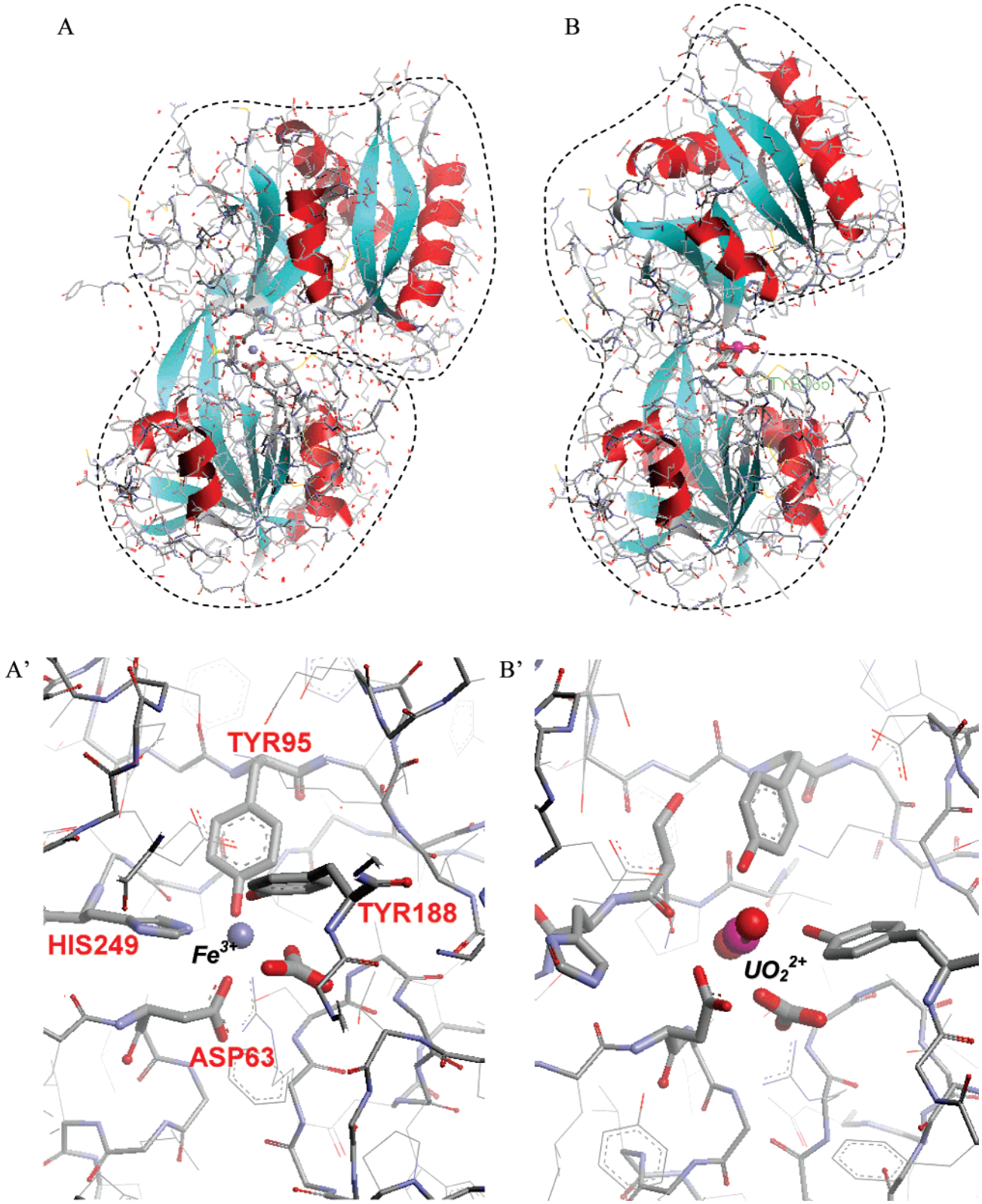

[a] (A and A′) Fe^{3+} N lobe of holotransferrin from PDB entry 1a8e and (B and B′) proposed model of uranyl-N lobe fulfilling all constraints drawn from experiments.

lobes seemed to be shifted simultaneously. This is in agreement with UV−visible spectroscopy results at 242 nm, where absorptivity increases displayed a single slope upon uranyl binding, suggesting a similar interaction with both sites. By reducing solvent access, domain closure should largely increase the thermal stability of the protein, but in the event of uranyl binding, T_m shifts are very small (~3.2 and ~2.3 °C) which seems incompatible with important conformational modification.

Simply to help our understanding and to take advantage of a strong body of analytical results, a scheme (Scheme 1) was drawn up from the available data using a semi-open

conformation of the protein N lobe fulfilling the tyrosine−uranyl binding and aspartate−uranyl proximity observed. The model structure obtained with side chain flexibility only was minimized in the Amber6 (*74*) force field using published uranyl parameters (*75*) and deprotonated TYR parameters for Tyr95 and Tyr188 (*76*). Interestingly, the proximity between the His side chain and uranyl is not favored during minimization. Instead of the His side chain, a peptide carbonyl points toward UO_2. Although this model is only a hypothetical structure, it shows a coherent picture between the coordination sphere of UO_2^{2+} and a partially open conformation. Our data converge to indicate that the uranyl-TF remains in a partially open conformation upon UO_2^{2+} binding. As previously reported, bismuth or aluminum forms stable complexes with transferrin, but the competitions for the transferrin receptor were in favor of iron (*77*, *78*). In the particular case of bismuth therapy, where large amounts of bismuth salts are daily injected, the authors did not discard the possibility of high bismuth−transferrin complex concentrations, and possible interactions with the receptor. Given the data we obtained with K562 cells, a relative concentration ratio of uranyl-TF to holoTF of more than 20 should be present in the blood to produce a significant transport via the TF receptor, which cannot be achieved in vivo.

In conclusion, the experimental data presented in this work show that uranyl-TF cannot adopt the appropriate conformation for optimal binding to its receptor. Consequently, although TF may be a significant UO_2^{2+} shuttle in the blood, UO_2^{2+} intake in target organs cannot result from uranyl transfer through the transferrin receptor-mediated pathway. Determining the entrance pathway of UO_2 in the cells is therefore the next challenge to improve our understanding uranium toxicity.

ACKNOWLEDGMENT

We thank Dr. M. Desmadril and E. Mintz for helpful discussions in thermodynamic and circular dichroism results. This work was supported by the Nuclear Toxicology program of CEA.

REFERENCES

1. Taylor, D. M., and Taylor, S. K. (1997) Environmental uranium and human health, *Rev. Environ. Health 12*, 147−157.
2. Wrenn, M. E., Bertelli, P. W., Durbin, N. P., Lipsztein, J. L., and Eckerman, K. F. (1994) A comprehensive metabolic model for uranium metabolism and dosimetry based on human and animal data, *Radiat. Prot. Dosim. 53*, 255−258.
3. Agency for Toxic Substances and Disease Registry (ATSDR) (1999) Toxicological profile for uranium, ATSDR, Atlanta.
4. McClain, D. E., Benson, K. A., Dalton, T. K., Ejnik, J., Emond, C. A., Hodge, S. J., Kalinich, J. F., Landauer, M. A., Miller, A. C., Pellmar, T. C., Stewart, M. D., Villa, V., and Xu, J. (2001) Biological effects of embedded depleted uranium (DU): Summary of armed forces radiobiology research institute research, *Sci. Total Environ. 274*, 115−118.
5. Kurttio, P., Auvinen, A., Salonen, L., Saha, H., Pekkanen, J., Makelainen, I., Vaisanen, S. B., Penttila, I. M., and Komulainen, H. (2002) Renal effects of uranium in drinking water, *Environ. Health Perspect. 110*, 337−342.
6. Leggett, R. W., and Pellmar, T. C. (2003) The biokinetics of uranium migrating from embedded DU fragments, *J. Environ. Radioact. 64*, 205−225.
7. Lemercier, V., Millot, X., Ansoborlo, E., Menetrier, F., Flury-Herard, A., Rousselle, C., and Scherrmann, J. M. (2003) Study of uranium transfer across the blood-brain barrier, *Radiat. Prot. Dosim. 105*, 243−245.
8. Kurttio, P., Komulainen, H., Leino, A., Salonen, L., Auvinen, A., and Saha, H. (2005) Bone as a possible target of chemical toxicity of natural uranium in drinking water, *Environ. Health Perspect. 113*, 68−72.
9. Scapolan, S. E. A., Moulin, C., and Madic, C. (1998) Investigations by time-resolved laser-induced fluorescence and capillary electrophoresis of the uranyl-phosphate species: Application to blood serum, *J. Alloys Compd.*, 106−111.
10. Scapolan, S. E. A., Moulin, C., and Madic, C. (1998) Uranium-(VI)-transferrin system studied by time-resolved laser induced fluorescence, *Radiat. Prot. Dosim. 79*, 505−508.
11. Taylor, D. M. (1998) The bioinorganic chemistry of actinides in blood, *J. Alloys Compd. 271*, 6−10.
12. Vidaud, C., Dedieu, A., Basset, C., Plantevin, S., Dany, I., Pible, O., and Quemeneur, E. (2005) Screening of human serum proteins for uranium binding, *Chem. Res. Toxicol. 18*, 946−953.
13. Llorens, I., Den Auwer, C., Moisy, P., Ansoborlo, E., Vidaud, C., and Funke, H. (2005) Neptunium uptake by serum transferring, *FEBS Lett. 272*, 1739−1744.
14. Grossmann, J. G., Neu, M., Evans, R. W., Lindley, P. F., Appel, H., and Hasnain, S. S. (1993) Metal-induced conformational changes in transferrins, *J. Mol. Biol. 229*, 585−590.
15. Grossmann, J. G., Crawley, J. B., Strange, R. W., Patel, K. J., Murphy, L. M., Neu, M., Evans, R. W., and Hasnain, S. S. (1998) The nature of ligand-induced conformational change in transferrin in solution. An investigation using X-ray scattering, XAFS and site-directed mutants, *J. Mol. Biol. 279*, 461−472.
16. Sun, H. L. H., and Sadler, P. J. (1999) Transferrin as a metal ion mediator, *Chem. Rev. 99*, 2817−2842.
17. Jeffrey, P. D., Bewley, M. C., MacGillivray, R. T., Mason, A. B., Woodworth, R. C., and Baker, E. N. (1998) Ligand-induced conformational change in transferrins: Crystal structure of the open form of the N-terminal half-molecule of human transferring, *Biochemistry 37*, 13978−13986.
18. Hirose, M. (2000) The structural mechanism for iron uptake and release by transferrins, *Biosci., Biotechnol., Biochem. 64*, 1328−1336.
19. Adams, T. E., Mason, A. B., He, Q. Y., Halbrooks, P. J., Briggs, S. K., Smith, V. C., MacGillivray, R. T., and Everse, S. J. (2003) The position of arginine 124 controls the rate of iron release from the N-lobe of human serum transferrin. A structural study, *J. Biol. Chem. 278*, 6027−6033.
20. Nicholson, H., Anderson, B. F., Bland, T., Shewry, S. C., Tweedie, J. W., and Baker, E. N. (1997) Mutagenesis of the histidine ligand in human lactoferrin: Iron binding properties and crystal structure of the histidine-253 → methionine mutant, *Biochemistry 36*, 341−346.
21. Mizutani, K., Yamashita, H., Kurokawa, H., Mikami, B., and Hirose, M. (1999) Alternative structural state of transferrin. The crystallographic analysis of iron-loaded but domain-opened ovotransferrin N-lobe, *J. Biol. Chem. 274*, 10190−10194.
22. Peterson, N. A., Anderson, B. F., Jameson, G. B., Tweedie, J. W., and Baker, E. N. (2000) Crystal structure and iron-binding properties of the R210K mutant of the N-lobe of human lactoferrin: Implications for iron release from transferrins, *Biochemistry 39*, 6625−6633.
23. Baker, H. M., He, Q. Y., Briggs, S. K., Mason, A. B., and Baker, E. N. (2003) Structural and functional consequences of binding site mutations in transferrin: Crystal structures of the Asp63Glu and Arg124Ala mutants of the N-lobe of human transferring, *Biochemistry 42*, 7084−7089.
24. Wally, J., Halbrooks, P. J., Vonrhein, C., Rould, M. A., Everse, S. J., Mason, A. B., and Buchanan, S. K. (2006) The crystal structure of iron-free human serum transferrin provides insight into inter-lobe communication and receptor binding, *J. Biol. Chem. 281*, 24934−24944.
25. Harris, W. R. (1998) Binding and transport of nonferrous metals by serum transferring, *Struct. Bonding 92*, 121−162.
26. Gumerov, D. R., Mason, A. B., and Kaltashov, I. A. (2003) Interlobe communication in human serum transferrin: Metal binding and conformational dynamics investigated by electrospray ionization mass spectrometry, *Biochemistry 42*, 5421−5428.
27. Mason, A. B., Halbrooks, P. J., James, N. G., Connolly, S. A., Larouche, J. R., Smith, V. C., MacGillivray, R. T., and Chasteen, N. D. (2005) Mutational analysis of C-lobe ligands of human serum transferrin: Insights into the mechanism of iron release, *Biochemistry 44*, 8013−8021.
28. Aisen, P. (1998) Transferrin, the Transferrin Receptor, and the Uptake of Iron by Cells, *Met. Ions Biol. Syst. 35*, 585−631.

29. Baker, H. M., Anderson, B. F., and Baker, E. N. (2003) Dealing with iron: Common structural principles in proteins that transport iron and heme, *Proc. Natl. Acad. Sci. U.S.A. 100*, 3579−3583.
30. Bennett, M. J., Lebron, J. A., and Bjorkman, P. J. (2000) Crystal structure of the hereditary haemochromatosis protein HFE complexed with transferrin receptor, *Nature 403*, 46−53.
31. Giannetti, A. M., and Bjorkman, P. J. (2004) HFE and transferrin directly compete for transferrin receptor in solution and at the cell surface, *J. Biol. Chem. 279*, 25866−25875.
32. Giannetti, A. M., Snow, P. M., Zak, O., and Bjorkman, P. J. (2003) Mechanism for multiple ligand recognition by the human transferrin receptor, *PLoS Biol. 1*, E51.
33. Grossmann, J. G., Mason, A. B., Woodworth, R. C., Neu, M., Lindley, P. F., and Hasnain, S. S. (1993) Asp ligand provides the trigger for closure of transferrin molecules. Direct evidence from X-ray scattering studies of site-specific mutants of the N-terminal half-molecule of human transferring, *J. Mol. Biol. 231*, 554−558.
34. Mason, A., He, Q. Y., Tam, B., MacGillivray, R. A., and Woodworth, R. (1998) Mutagenesis of the aspartic acid ligands in human serum transferrin: Lobe-lobe interaction and conformation as revealed by antibody, receptor-binding and iron-release studies, *Biochem. J. 330* (Part 1), 35−40.
35. Sun, H., Li, H., Mason, A. B., Woodworth, R. C., and Sadler, P. J. (1999) N-Lobe versus C-lobe complexation of bismuth by human transferring, *Biochem. J. 337* (Part 1), 105−111.
36. Hemadi, M., Kahn, P. H., Miquel, G., and El Hage Chahine, J. M. (2004) Transferrin's mechanism of interaction with receptor 1, *Biochemistry 43*, 1736−1745.
37. Aisen, P. (2004) Transferrin receptor 1, *Int. J. Biochem. Cell Biol. 36*, 2137−2143.
38. Cheng, Y., Zak, O., Aisen, P., Harrison, S. C., and Walz, T. (2004) Structure of the human transferrin receptor-transferrin complex, *Cell 116*, 565−576.
39. Xu, G., Liu, R., Zak, O., Aisen, P., and Chance, M. R. (2005) Structural allostery and binding of the transferrin*receptor complex, *Mol. Cell. Proteomics 4*, 1959−1967.
40. Taylor, D. (1993) Transferrin complexes with non-physiological and toxic metals, *Perspect. Bioinorg. Chem. 2*, 139−159.
41. Li, H., Sadler, P. J., and Sun, H. (1996) Rationalization of the strength of metal binding to human serum transferring, *Eur. J. Biochem. 242*, 387−393.
42. Messori, L., Poggetto, G. D., Monnanni, R., and Hirose, J. (1997) The pH dependent properties of metallotransferrins: A comparative study, *BioMetals 10*, 303−313.
43. Harris, W. R., Yang, B., Abdollahi, S., and Hamada, Y. (1999) Steric restrictions on the binding of large metal ions to serum transferring, *J. Inorg. Biochem. 76*, 231−242.
44. Halbrooks, P. J., Giannetti, A. M., Klein, J. S., Bjorkman, P. J., Larouche, J. R., Smith, V. C., MacGillivray, R. T., Everse, S. J., and Mason, A. B. (2005) Composition of pH-sensitive triad in C-lobe of human serum transferrin. Comparison to sequences of ovotransferrin and lactoferrin provides insight into functional differences in iron release, *Biochemistry 44*, 15451−15460.
45. Tinoco, A. D., and Valentine, A. M. (2005) Ti(IV) binds to human serum transferrin more tightly than does Fe(III), *J. Am. Chem. Soc. 127*, 11218−11219.
46. Battistuzzi, G., Calzolai, L., Messori, L., and Sola, M. (1995) Metal-induced conformational heterogeneity of transferrins: A spectroscopic study of indium(III) and other metal(III)-substituted transferrins, *Biochem. Biophys. Res. Commun. 206*, 161−170.
47. Zhang, M., Gumerov, D. R., Kaltashov, I. A., and Mason, A. B. (2004) Indirect detection of protein-metal binding: Interaction of serum transferrin with In^{3+} and Bi^{3+}, *J. Am. Soc. Mass Spectrom. 15*, 1658−1664.
48. Beatty, E. J., Cox, M. C., Frenkiel, T. A., Tam, B. M., Mason, A. B., MacGillivray, R. T., Sadler, P. J., and Woodworth, R. C. (1996) Interlobe communication in ^{13}C-methionine-labeled human transferring, *Biochemistry 35*, 7635−7642.
49. Madic, C. In *Chimie des Actinides, Chimie Théorique et Modélisation*, Chapter VII, Rapport sur la Science et la Technologie, Académie des Science: Paris, 2000, pp 185−195.
50. Mirto, H., Henge-Napoli, M. H., Gibert, R., Ansoborlo, E., Fournier, M., and Cambar, J. (1999) Intracellular behaviour of uranium(VI) on renal epithelial cell in culture (LLC-PK1): Influence of uranium speciation, *Toxicol. Lett. 104*, 249−256.
51. Carriere, M., Avoscan, L., Collins, R., Carrot, F., Khodja, H., Ansoborlo, E., and Gouget, B. (2004) Influence of uranium speciation on normal rat kidney (NRK-52E) proximal cell cytotoxicity, *Chem. Res. Toxicol. 17*, 446−452.
52. Sutton, M., and Burastero, S. R. (2004) Uranium(VI) solubility and speciation in simulated elemental human biological fluids, *Chem. Res. Toxicol. 17*, 1468−1480.
53. Gourion-Arsiquaud, S., Chevance, S., Bouyer, P., Garnier, L., Montillet, J. L., Bondon, A., and Berthomieu, C. (2005) Identification of a Cd^{2+}- and Zn^{2+}-binding site in cytochrome c using FTIR coupled to an ATR microdialysis setup and NMR spectroscopy, *Biochemistry 44*, 8652−8663.
54. Chasteen, N. D., White, L. K., and Campbell, R. F. (1977) Metal site conformational states of vanadyl(IV) human serotransferrin complexes, *Biochemistry 16*, 363−365.
55. Du, X. L., Zhang, T. L., Yuan, L., Zhao, Y. Y., Li, R. C., Wang, K., Yan, S. C., Zhang, L., Sun, H., and Qian, Z. M. (2002) Complexation of ytterbium to human transferrin and its uptake by K562 cells, *Eur. J. Biochem. 269*, 6082−6090.
56. Messori, L., Orioli, P., Banholzer, V., Pais, I., and Zatta, P. (1999) Formation of titanium(IV) transferrin by reaction of human serum apotransferrin with titanium complexes, *FEBS Lett. 442*, 157−161.
57. Vidaud, C., Pible, O., and Quemeneur, E. (2002) Protein targets of toxic hard Lewis metals, *Recent Res. Dev. Biochem. 3*, 511−525.
58. Zak, O., and Aisen, P. (1988) Spectroscopic and thermodynamic studies on the binding of gadolinium(III) to human serum transferring, *Biochemistry 27*, 1075−1080.
59. Venyaminov, S., and Kalnin, N. N. (1990) Quantitative IR spectrophotometry of peptide compounds in water (H_2O) solutions. II. Amide absorption bands of polypeptides and fibrous proteins in α-, β-, and random coil conformations, *Biopolymers 30*, 1259−1271.
60. Chirgadze, Y. N., Fedorov, O. V., and Trushina, N. P. (1975) Estimation of amino acid residue side-chain absorption in the infrared spectra of protein solutions in heavy water, *Biopolymers 14*, 679−694.
61. Venyaminov, S., and Kalnin, N. N. (1990) Quantitative IR spectrophotometry of peptide compounds in water (H_2O) solutions. I. Spectral parameters of amino acid residue absorption bands, *Biopolymers 30*, 1243−1257.
62. Susi, H. (1969) *Structure and Stability of Biological Macromolecules*, Vol. 2, Dekker, New York.
63. Hienerwadel, R., and Berthomieu, C. (1995) Bicarbonate binding to the non-heme iron of photosystem II investigated by Fourier transform infrared difference spectroscopy and ^{13}C-labeled bicarbonate, *Biochemistry 34*, 16288−16297.
64. Noguchi, T., Inoue, Y., and Tang, X. S. (1999) Hydrogen bonding interaction between the primary quinone acceptor QA and a histidine side chain in photosystem II as revealed by Fourier transform infrared spectroscopy, *Biochemistry 38*, 399−403.
65. Socrates, G. (1994) *Infrared Characteristic Group Frequencies*, John Wiley & Sons, Inc., New York.
66. Nakamoto, K. (1997) *Infrared and Raman spectra of inorganic and coordination compounds. Part B: Application in coordination, organometallic, and biochemistry*, John Wiley & Sons, Inc., New York.
67. Tang, S., MacColl, R., and Parsons, P. J. (1995) Spectroscopic study of the interaction of aluminum ions with human transferring, *J. Inorg. Biochem. 60*, 175−185.
68. Lin, L. N., Mason, A. B., Woodworth, R. C., and Brandts, J. F. (1994) Calorimetric studies of serum transferrin and ovotransferrin. Estimates of domain interactions, and study of the kinetic complexities of ferric ion binding, *Biochemistry 33*, 1881−1888.
69. Lin, L. N., Mason, A. B., Woodworth, R. C., and Brandts, J. F. (1993) Calorimetric studies of the N-terminal half-molecule of transferrin and mutant forms modified near the Fe^{3+}-binding site, *Biochem. J. 293* (Part 2), 517−522.
70. Brewer, J. M., and Wampler, J. E. (2001) A differential scanning calorimetric study of the effects of metal ions, substrate/product, substrate analogues and chaotropic anions on the thermal denaturation of yeast enolase 1, *Int. J. Biol. Macromol. 28*, 213−218.
71. He, Q. Y., Mason, A. B., Pakdaman, R., Chasteen, N. D., Dixon, B. K., Tam, B. M., Nguyen, V., MacGillivray, R. T., and Woodworth, R. C. (2000) Mutations at the histidine 249 ligand profoundly alter the spectral and iron-binding properties of human serum transferrin N-lobe, *Biochemistry 39*, 1205−1210.
72. MacGillivray, R. T., Bewley, M. C., Smith, C. A., He, Q. Y., Mason, A. B., Woodworth, R. C., and Baker, E. N. (2000) Mutation of the iron ligand His 249 to Glu in the N-lobe of human

transferrin abolishes the dilysine "trigger" but does not significantly affect iron release, *Biochemistry 39*, 1211−1216.
73. Xu, G., Liu, R., Zak, O., Aisen, P., and Chance, M. R. (2005) Structural Allostery and Binding of the Transferrin·Receptor Complex, *Mol. Cell. Proteomics 4*, 1959−1967.
74. Case, D. A., Pearlman, D. A., Caldwell, J. W., Cheatham, I. T. E., Ross, W. S., Simmerling, C. L., Darden, T. A., Merz, K. M., Stanton, R. V., Cheng, A. L., Vincent, J. J., Crowley, M., Tsui, V., Radmer, V., Duan, Y., Pitera, J., Massova, I., Seibel, G. L., Singh, U. C., Weiner, P. K., and Kollman, P. A. (1999) *Amber6*, University of California, San Francisco.
75. Guilbaud, P., and Wipff, G. (1996) Force field representation of the UO_2^{2+} cation from free energy MD simulations in water. Tests on its 18-crown-6 and NO_3-adducts, and on its calix[6]arene^{6-} and CMPO complexes, *THEOCHEM 366*, 55−63.
76. Pible, O., Guilbaud, P., Pellequer, J. L., Vidaud, C., and Quemeneur, E. (2006) Structural insights into protein-uranyl interaction: Towards an in silico detection method. *Biochimie* (in press).
77. Miquel, G., Nekaa, T., Kahn, P. H., Hemadi, M., and El Hage Chahine, J. M. (2004) Mechanism of formation of the complex between transferrin and bismuth, and interaction with transferrin receptor 1, *Biochemistry 43*, 14722−14731.
78. Hemadi, M., Miquel, G., Kahn, P. H., and El Hage Chahine, J. M. (2003) Aluminum exchange between citrate and human serum transferrin and interaction with transferrin receptor 1, *Biochemistry 42*, 3120−3130.

BI061945H